

Evidence accumulation determines conscious access

Michael Pereira^{1,2,3}, Pierre Megevand^{4,5,6}, Mi Xue Tan¹, Wenwen Chang¹, Shuo Wang^{3,7}, Ali Rezai³, Margitta Seeck⁴, Marco Corniola^{8,9}, Shahran Momjian^{8,9}, Fosco Bernasconi¹, Olaf Blanke^{1,9,+}, Nathan Faivre^{1,2,*}

Affiliations

1 Laboratory of Cognitive Neuroscience, Center for Neuroprosthetics and Brain Mind Institute, Faculty of Life Sciences, Swiss Federal Institute of Technology (EPFL), Geneva, Switzerland

2 Université Grenoble Alpes, CNRS, LPNC UMR 5105, Grenoble, France

3 Rockefeller Neuroscience Institute (RNI), West Virginia University, Morgantown, United States

4 Neurology Division, Department of Clinical Neuroscience, Geneva University Hospitals, Geneva, Switzerland

5 Department of Fundamental Neuroscience, University of Geneva, Geneva, Switzerland

6 Wyss Center for Bio and Neuroengineering, Geneva, Switzerland

7 Department of Chemical and Biomedical Engineering, West Virginia University, Morgantown, United States

8 Neurosurgery Division, Department of Clinical Neuroscience, University of Geneva University Hospitals, Geneva, Switzerland

9 Faculty of Medicine, University Hospital Geneva, Geneva, Switzerland

+ equal contribution

* Corresponding author:

Nathan Faivre

Laboratoire de Psychologie et Neurocognition

CNRS UMR 5105

UGA BSHM

1251 Avenue Centrale

38058 Grenoble Cedex 9

Acknowledgments: MP is supported by an Early Postdoc.Mobility fellowship from the Swiss National Science Foundation (P2ELP3_187974). PM is supported by an Ambizione fellowship from the Swiss National Science Foundation (PZ00P3_167836). MS is supported by grants from the Swiss National Science Foundation (163398, 80365) and Fondation Privé. OB is supported by the Bertarelli Foundation, the Swiss National Science Foundation, and the European Science Foundation. NF has received funding from the European Research Council (ERC) under the European Union's Horizon 2020 research and innovation programme (Grant agreement No. 803122). We acknowledge support from the Wyss Center for Bio and Neuroengineering and the Epileptology Unit, Division of Neurology, Geneva University Hospitals. We thank Jean-Baptiste Eichenlaub, Vincent de Gardelle, Emanuela de Falco, Liad Mudrik and Adam Shai for their comments.

Author Contributions: MP, MT, and NF developed the study concept and contributed to the study design. PM and MS developed the clinical trial that generated the microelectrode array data. Data collection and data analysis were performed by MP, PM, FB, MT, WC, and NF. MP performed modelling work. MC and SM performed surgery. MP and NF drafted the paper; all authors provided critical revisions and approved the final version of the paper for submission.

Keywords: tactile perception, consciousness, confidence, metacognition, Utah array, single-unit activity, evidence accumulation

The authors declare no competing interests.

Data and code availability statement: Behavioral, electrocorticographic and electroencephalographic data with the corresponding analyses scripts will be made available upon publication. Single-neuron data are available upon request.

1 A fundamental scientific question concerns the neuronal basis of perceptual
2 consciousness, which encompasses the perceptual experience and reflexive monitoring
3 associated with a sensory event. Although recent human studies identified individual
4 neurons reflecting stimulus visibility, their functional role for perceptual consciousness
5 remains unknown. Here, we provide neuronal and computational evidence indicating that
6 perceptual and reflexive consciousness are governed by an all-or-none process
7 involving accumulation of perceptual evidence. We recorded single-neuron activity in a
8 participant with a microelectrode implant in the posterior parietal cortex, considered a
9 substrate for evidence accumulation, while he detected vibrotactile stimuli around
10 detection threshold and provided confidence estimates. We found that detected stimuli
11 elicited firing rate patterns resembling evidence accumulation during decision-making,
12 irrespective of response effectors. Similar neurons encoded the intensity of task-
13 irrelevant stimuli, suggesting their role for consciousness per se, irrespective of report.
14 We generalized these findings in healthy volunteers using electroencephalography and
15 reproduced their behavioral and neural responses with a computational model. This
16 model considered stimulus detection if accumulated evidence reached a bound, and
17 confidence as the distance between maximal evidence and that bound. Applying this
18 mechanism to our neuronal data, we were able to decode single-trial confidence ratings
19 both for detected and undetected stimuli. Our results show that the specific gradual
20 changes in neuronal dynamics during evidence accumulation govern perceptual
21 consciousness and reflexive monitoring in humans.

22 The processing of sensory signals by the human brain gives rise to two interrelated phenomena:
23 perceptual consciousness, defined as the subjective experience associated with a sensory
24 event (Chalmers, 1995; Nagel, 1974; Block 2011), and perceptual monitoring, defined as the
25 capacity to introspect and reflect upon the subjective experience associated with a sensory
26 event (Flavell, 1979; Koriat, 2006; Fleming, Dolan, and Frith 2012). The main strategy employed
27 to study conscious processing consists in relating first-order subjective reports to neural activity
28 to identify the minimal set of neuronal events and mechanisms sufficient for a specific conscious
29 percept (i.e., neural correlates of consciousness or NCCs : Koch et al., 2016). To identify NCCs,
30 most experimental paradigms have adopted a contrastive approach, whereby distinct
31 phenomenal experiences induced by constant sensory stimulation are compared (Baars, 1998).
32 One of the simplest contrasts is obtained when stimuli are presented at low intensity or
33 embedded in noise so that only a certain proportion of them is detected (Dehaene et al., 2006).
34 A comparison of neural activity elicited by detected and missed stimuli allows distinguishing the
35 neural correlates of conscious vs. unconscious sensory processing, and therefore identifying
36 NCCs given that specific confounds are ruled out (Aru et al., 2012). However, although rare
37 investigations in humans have described single neurons in the temporal lobe encoding stimulus
38 detection (Quiroga et al., 2008; Reber et al., 2017), the mechanistic role of neuronal activity for

39 perceptual consciousness remains unknown. One prominent theory of consciousness, the
40 global neuronal workspace, proposes that a stimulus is consciously perceived when its
41 corresponding neural activity is globally broadcasted across the cortex (Mashour, et al., 2020).
42 This theory assumes that this global broadcast is triggered when an (unconscious) evidence
43 accumulation process reaches a threshold (Dehaene et al., 2014; Dehaene, 2009; Shadlen
44 2011), similar to the physiological processes underlying decision-making (Bollimunta & Ditterich,
45 2012; Katz et al., 2016; Roitman & Shadlen, 2002; Zhou & Freedman, 2019). Although various
46 neuroimaging studies have interpreted increases in neural activity elicited by detected stimuli
47 (versus missed stimuli) as evidence accumulation (Salti et al., 2015; Tagliabue et al., 2019;
48 Wyart & Tallon-Baudry, 2009), little empirical evidence supports an evidence accumulation
49 account of perceptual consciousness, especially at the single neuron level.

50 Besides perceptual consciousness, the main strategy to study perceptual monitoring consists in
51 assessing how second-order reports like confidence judgments co-vary with the accuracy of a
52 given perceptual task (first-order reports; Fleming & Lau, 2014). As most studies investigating
53 perceptual monitoring rely on first-order discrimination tasks with stimuli that are always
54 detected, less is known regarding how the brain monitors the presence or absence of subjective
55 experience (Li et al., 2014; Mazor et al., 2020). Moreover, the interdependencies between
56 perceptual consciousness and monitoring remain to be described empirically: while some
57 theories of consciousness argue that conscious access requires a higher order representation
58 of a stimulus (Brown et al., 2019; Lau & Rosenthal, 2011), or necessarily comes with a sense of
59 confidence (Shea & Frith, 2019), other theories argue that first-order representations may be
60 sufficient (Lamme, 2010; Zeki, 2007). Like for perceptual consciousness, several models
61 propose that evidence accumulation plays an important role for the formation of perceptual
62 confidence (Kvam et al., 2015; Pereira et al., 2020; Pleskac & Busemeyer, 2010; van den Berg
63 et al., 2016). Yet, to our knowledge the underlying neural mechanisms remain to be described.

64 Here, we sought to investigate the role of evidence accumulation in perceptual consciousness
65 and perceptual monitoring by asking participants to detect weak vibrotactile stimuli and rate their
66 confidence in having detected them. We reasoned that both detection and confidence underlie
67 decision-making processes whereby participants accumulate perceptual evidence over time and
68 gauge its level relative to decision criteria. We examined this possibility in a patient implanted
69 with a microelectrode array in the posterior parietal cortex (PPC, Fig. 1A), considered as one of
70 the functional hotspots of evidence accumulation in the non-human primate brain (Bollimunta &

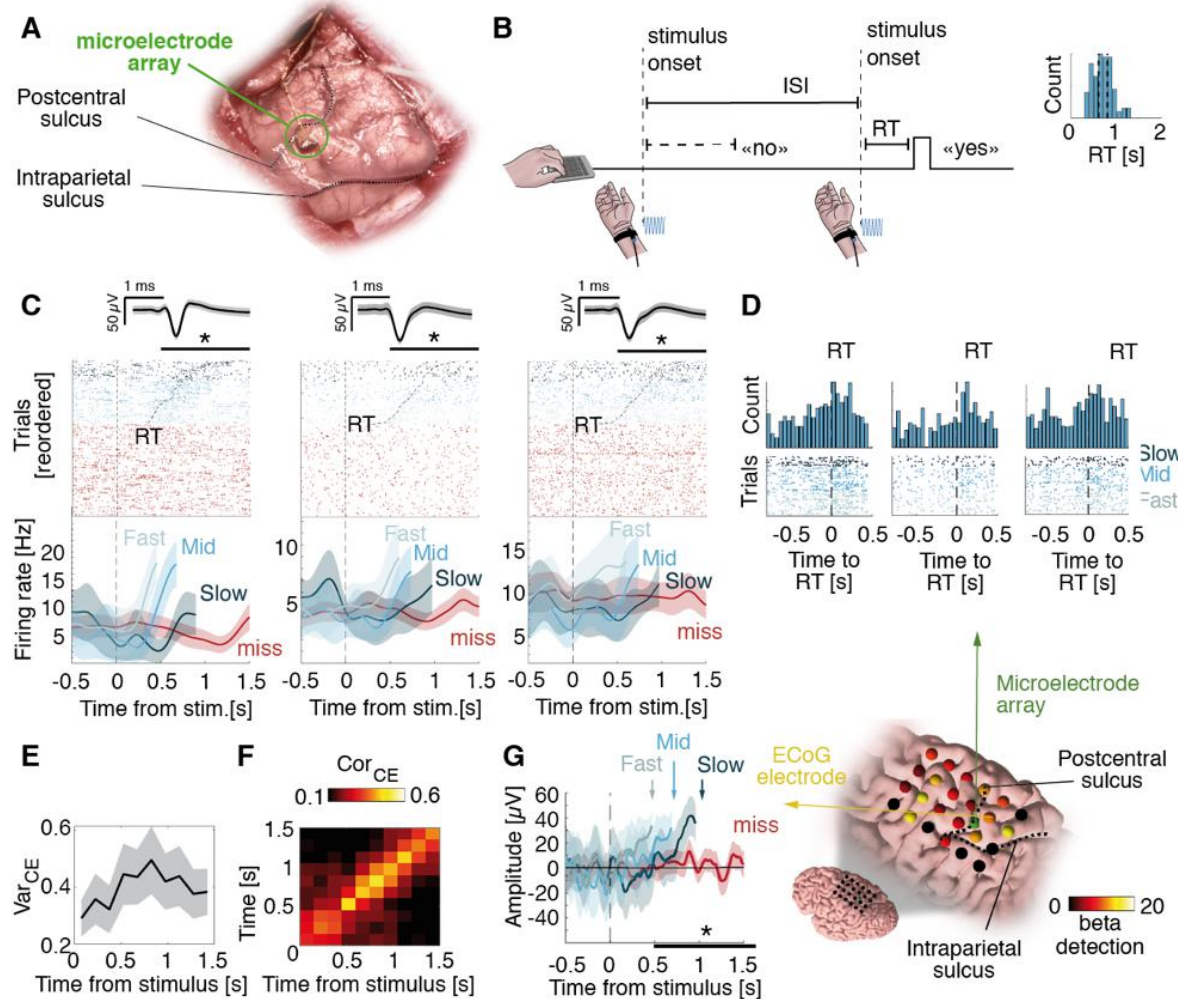
71 Ditterich, 2012; Gold & Shadlen, 2007; Katz et al., 2016; Roitman & Shadlen, 2002; Zhou &
72 Freedman, 2019). We isolated 368 putative single neurons (Fig. S1) in three different
73 experiments with immediate, delayed, and no-responses in order to characterize the neural
74 correlates of detection and confidence at the single-neuron and population levels and link
75 evidence accumulation in the PPC to perceptual consciousness irrespective of response
76 effectors. These results were generalized in a fourth experiment involving a group of healthy
77 volunteers in whom we recorded scalp electroencephalography, perceptual consciousness and
78 monitoring responses while they detected the same vibrotactile stimuli. In a final step, we test
79 and propose an evidence accumulation computational model that reproduced the behavioral
80 and neural markers of both detection and confidence. Together, these results indicate that
81 subjective reports of perceptual consciousness and monitoring involve a common mechanism of
82 evidence accumulation orchestrated by the PPC.

83 Results

84 **Experiment 1: immediate-response task**

85 In *Experiment 1*, the participant was asked to detect vibrotactile stimuli applied to the right wrist
86 (contralateral to the PPC implant) with an intensity around detection threshold. Responses were
87 provided by a keypress with the left hand, immediately after perceiving a stimulus. A trial was
88 considered a hit when the participant responded within 2 s following stimulus onset (41.20% of
89 trials; mean response time (RT) and 95% confidence interval: 0.71 ± 0.02 s), otherwise, it was
90 considered a miss (58.80% of trials Fig. 1B). The participant rarely responded “yes” in the
91 absence of stimuli (0.36%; false-alarms), indicative of conservative behavior. We found 94/186
92 detection-selective neurons (50.54%; $p = 0.001$, Poisson GLM with permutation test across
93 neurons) with spike counts explained by detection (yes/no responses) between 0.5 to 1.5 s after
94 the stimulus onset. Some neurons were characterized by a hallmark of evidence accumulation
95 where increases in firing rates preceded detection reports depending on their response times
96 (Bollimunta & Ditterich, 2012; Katz et al., 2016; Roitman & Shadlen, 2002; Zhou & Freedman,
97 2019): the cumulative sum of spikes following stimulus onset correlated with the corresponding
98 RT in 67/94 detection-selective neurons (71.28%; $p = 0.001$; Fig. 1C) with some neurons
99 showing gradually increasing spike counts prior to the keypress (Fig. 1D). To further support
100 that increased spike counts represent an evidence accumulation process, we verified that the
101 proportion of variance not attributed to the point process increased after stimulus onset (Fig. 1E)
102 and that the corresponding covariance decayed with increasing time lag (Fig. 1F), in line with

103 what is expected for a diffusion process (Churchland et al., 2011). Finally, we replicated the
 104 increase in firing rate with electrocorticography (ECoG) by showing that the strongest effect of
 105 detection was localized in the PPC and pre-central gyrus (Fig. 1G). To summarize, we
 106 uncovered individual neurons in the human PPC with firing rates ramping up prior to detection
 107 reports, consistent with evidence accumulation.



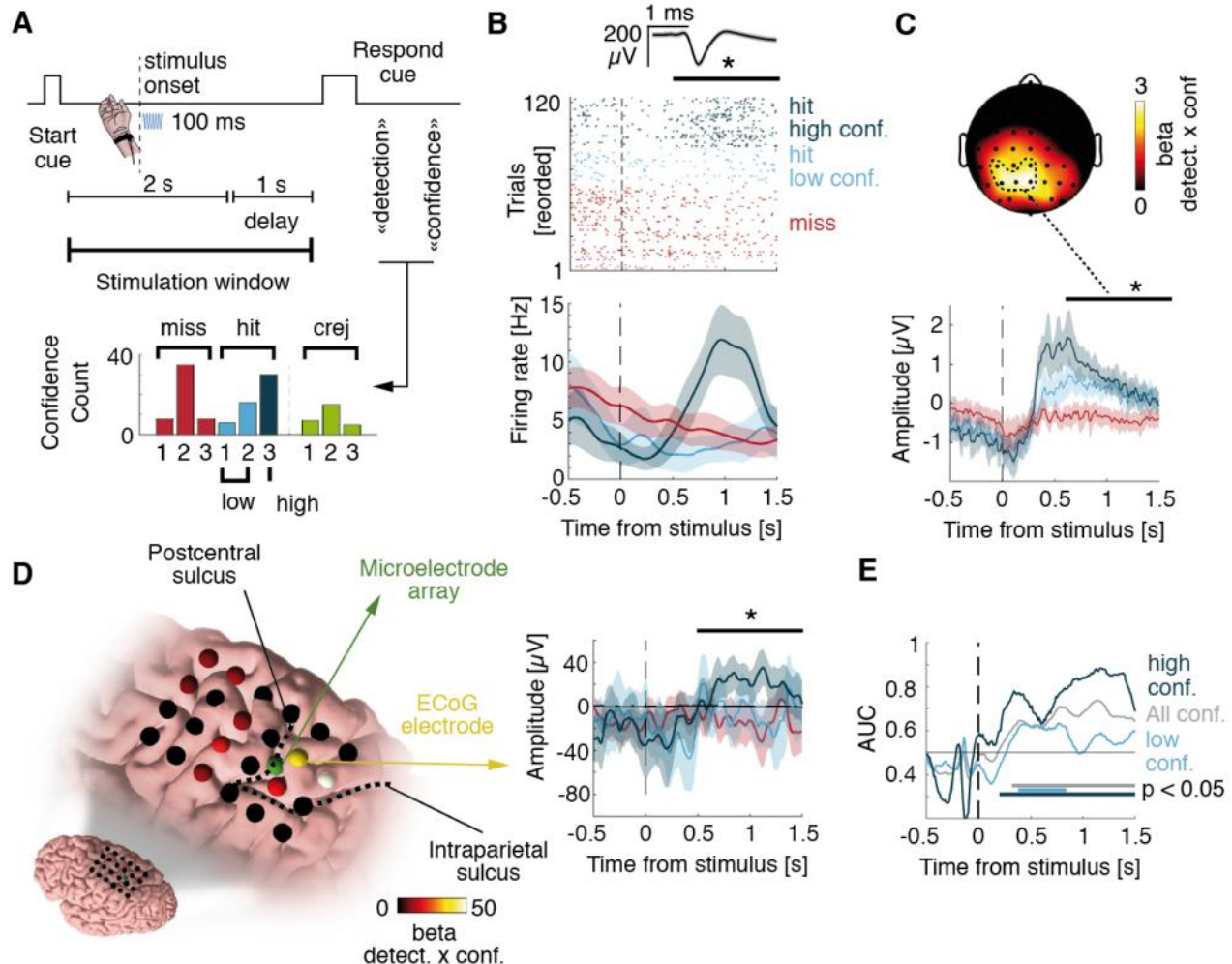
108 *Fig. 1. Neuronal correlates of detection in an immediate-response task (Experiment 1). (A)* Intraoperative photo of the
 109 *microelectrode array posterior to the postcentral sulcus and dorsal to the intraparietal sulcus. (B)* The participant
 110 *pressed a key as soon as he felt a stimulus (dashed vertical lines). In this example, the first stimulus is a miss (i.e. no*
 111 *key press within 2s following stimulus onset) and the second stimulus is a hit. ISI: inter-stimulus interval. Inset: RT*
 112 *distribution. (C) Example selective neurons with a latency effect for RT. Top: raster plot time-locked to stimulus onset*
 113 *with spike waveform and shaded standard deviation above. Hits were reordered according to RT (black dashed trace).*
 114 *Bottom: average firing rate for three terciles of RT (blue) and for misses (red). Statistics were performed on*
 115 *continuous data. (D) Top: RT-aligned spike count histograms for neurons in C (50 ms bins). Bottom: corresponding*
 116 *raster plots. (E) VarCE increases during the putative decision process for detection- and RT-selective neurons*
 117 *(N=47). Shaded areas represent 95%-confidence intervals (95%-CI) across selective neurons. (F) Corresponding*
 118 *analysis of covariance representing CorCE as heat maps, averaged across detection- and RT-selective neurons*
 119 *(N=47). (G) Left: Average ECoG response, aligned to stimulus onset from one electrode posterior to the*
 120 *microelectrode array for three terciles of RT. Right: ECoG grid with beta coefficients for detection. Non-significant*
 121 *electrodes are in black. All shaded areas represent 95%-CI and black horizontal bars represent the analysis window*
 122 *for statistics.*

123 **Experiment 2: delayed-response task**

124 Next, we tested whether neuronal responses relate to conscious perception irrespective of
125 motor actions by imposing a delay between stimulus onset and reports. We also assessed
126 whether the strength of these neuronal representations co-vary with reported confidence
127 (Rutishauser et al., 2015, 2018). In Experiment 2, we asked the participant to report vocally the
128 detection of the stimuli with a minimal delay of 1 s after stimulus onset (Fig. 2A, upper panel).
129 To assess the role of evidence accumulation for conscious monitoring, we also asked the
130 participant to vocally report his confidence (high, medium, low) in his response. Similar to
131 Experiment 1, 50.5% of stimuli were detected (hits) (20% trials had no stimuli, of which 5% were
132 false-alarms, confirming his conservative strategy). When a stimulus was presented, confidence
133 was higher following hits (2.46 ± 0.10) than misses (2.00 ± 0.08 ; $X^2 = 20.09$, $p = 4.3 \times 10^{-5}$),
134 indicative of accurate detection monitoring processes (Fig. 2A, lower panel).

135 We ran a factorial analysis to identify neurons encoding detection and/or confidence. We found
136 17/86 neurons showing an interaction between detection and confidence (19.77%, $p = 0.002$,
137 permutation test) driven by an increased firing rate for hits with high confidence (Fig. 2B). Only
138 one neuron showed only a main effect of detection (1.16%, $p = 0.57$) and two a main effect of
139 confidence (2.33%, $p = 0.88$). A similar interaction between detection and confidence was found
140 in ECoG electrodes surrounding the microelectrode array (Fig. 2D) and in
141 electroencephalography (EEG) signals from 18 healthy volunteers recruited from Experiment 4
142 (Fig. 2C), consistent with previous EEG studies (Herding et al., 2019; Tagliabue et al., 2019). To
143 characterize how neuronal population activity relates to detection and confidence, we trained
144 decoders on the firing rate of all neurons and evaluated them out-of-sample. We decoded hits
145 from misses better than chance for both high confidence (Fig. 2E; max. area under the curve
146 (AUC): 0.88, 1.16s after stimulus onset) and low confidence (max. AUC: 0.63 accuracy at 0.77
147 s). This indicates that although low confidence hits and misses were indistinguishable based on
148 individual neurons they could be discriminated at the population-level, which confirms that our
149 results were not driven by high-confidence trials only. Finally, the output of the best decoder (at
150 1.13 s) correlated with confidence for hits ($R = 0.59$; $p < 0.001$, permutation test) but not for
151 misses ($R = 0.16$; $p = 0.13$), confirming that the neuronal signal driving detection also explains
152 confidence for detected stimuli. Together, results from Experiments 1 and 2 show that PPC
153 neurons exhibit evidence accumulation behavior and encode detection and confidence reports
154 irrespective of motor actions and report effector (i.e., keypress in Experiment 1, voice in
155 Experiment 2). Of note, the latency of the evidence accumulation process we uncovered in

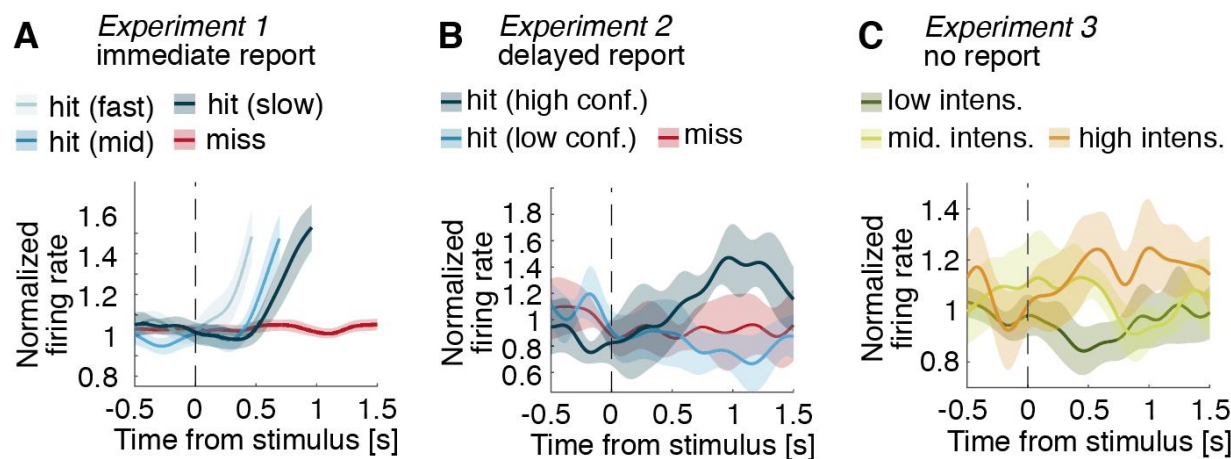
156 Experiment 2 is qualitatively compatible with the distribution of RTs measured in Experiment 1,
 157 which suggests that conscious access occurs with a delay of up to 1 s following weak
 158 vibrotactile stimulation.



159 *Fig.2. Neuronal correlates of detection and confidence in a delayed-response task (Experiment 2). (A)* Top:
 160 Vibrotactile stimuli were applied during a 2s window following an auditory cue. After 1s delay, the participant was
 161 prompted to give detection and confidence reports. Bottom: Distribution of confidence. For display purposes hereafter,
 162 signals corresponding to confidence values of 1 and 2 were merged into low-confidence, while confidence values of
 163 3 were considered as high-confidence. Statistics were done on the three levels. **(B)** Example selective neuron. Top:
 164 Raster plot time-locked to stimulus onset with spike waveform with shaded standard deviation above. Bottom:
 165 Corresponding firing rates. **(C)** EEG data showing a topographic map of beta coefficient for the interaction between
 166 detection and confidence for hits (dashed trace). The EEG amplitude time-locked to stimulus onset and averaged
 167 over 18 healthy controls is shown below. **(D)** Left: ECoG grid with beta coefficients for detection x confidence. Non-
 168 significant electrodes are in black. Right: Average ECoG amplitudes, aligned to stimulus onset from the electrode
 169 next to the microelectrode array **(E)** Decoding performance for different confidence levels. Horizontal lines show
 170 times of significant performance (permutation tests). All shaded areas represent 95%-CI and black horizontal bars
 171 represent the analysis window for statistics.

172 **Experiment 3: no-report paradigm**

173 To distinguish neuronal activity associated with subjective experience from activity associated
174 with subjective report (Aru et al., 2012; Pitts et al., 2014; Tsuchiya et al., 2015), in *Experiment 3*
175 we let the participant mind-wander while he was exposed to stimuli ranging between 0.5 to 5
176 times the perceptual-threshold intensity. We reasoned that neuronal activity would still encode
177 the intensity even for task-irrelevant stimuli if evidence accumulation determines conscious
178 perception beyond mere reports. While no behavioral task was enforced, we found that the
179 activity of 14/96 neurons increased with increasing stimulus intensity (14.58%, $p = 0.008$; Fig.
180 3C), similar to hits in Experiments 1-2 (Fig. 3A, B). The fact that stimulus intensity was
181 represented at the single-neuron level although the participant was not engaged in the task
182 argues against the possibility that our previous results in Experiments 1-2 reflected task activity
183 rather than perceptual processing leading to conscious access (Aru et al., 2012; Pitts et al.,
184 2014; Tsuchiya et al., 2015).



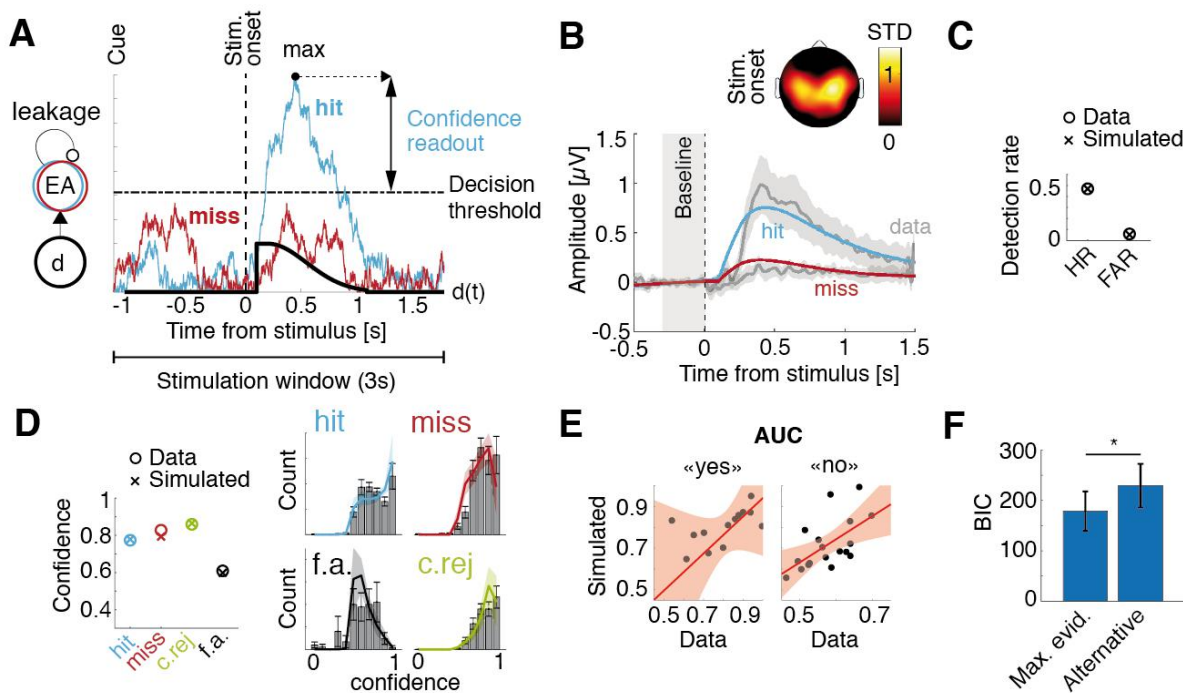
185 **Fig. 3.** Average firing rates of responsive neurons. Firing rates were normalized using a 0.3 s pre-stimulus baseline.
186 (A) Normalized firing rate for three bins of RT (hits; blue) and for misses (red), averaged across detection-selective
187 and RT-selective neurons with higher firing rates for hits ($N=47$). In Experiment 1, the participant answered with a
188 keypress for hits. (B) Normalized firing rate for high and low confidence for hits (blue) and for misses (red), averaged
189 across all detection- and confidence- selective neurons with higher firing rates for hits ($N=10$). In Experiment 2, the
190 participant waited at least one second before reporting detection and confidence vocally. (C) Normalized firing rate for
191 three bins of stimulus intensity, averaged across intensity-selective neurons ($N=14$). In Experiment 3, the participant
192 provided no detection or confidence report and was let to mind wander.

193 **Experiment 4: computational model of detection and confidence**

194 Informed by these human single-neuron data from Experiments 1-3, we sought to generalize
195 our decisional account of perceptual consciousness by identifying evidence accumulation
196 mechanisms underlying detection and confidence in EEG data (18 healthy volunteers, task
197 similar to Experiment 2). Participants behaved similarly to the aforementioned patient, with a
198 balanced number of hits and misses (Supplementary results) and EEG responses also showed
199 an interaction effect between detection and confidence (Fig. 2C). We developed an evidence
200 accumulation model to fit the behavioral and EEG data, assuming that participants attempted to
201 detect the stimulus by continuously accumulating evidence during a 3s stimulation window (from
202 trial onset until the response cue). To model the time uncertainty in our task (participants did not
203 know when a stimulus could be applied), we assumed that participants started accumulating
204 evidence before the stimulus onset (Devine et al., 2019). This was modelled as a null drift rate
205 across time except for a short-lasting boost triggered by the stimulus. A stimulus was perceived
206 if the simulated evidence accumulation (EA) process reached a bound (Kang et al., 2017) at any
207 time during the stimulus window (Fig. 4A), compatible with all-or-none views of conscious
208 access (Dehaene et al., 2014).

209 Confidence was read out from the distance between accumulated evidence and the decision
210 threshold (Pereira et al., 2020; Pleskac & Busemeyer, 2010). Importantly, we sampled
211 confidence when evidence reached a maximum across the stimulation window, which allowed
212 implementing a confidence readout for misses and correct rejections, for which no decision
213 threshold is crossed. To fit the model parameters to the data, we considered the shape of the
214 electrophysiological signature for hits and misses as a neural correlate of evidence
215 accumulation (O'Connell et al., 2012; Philiastides et al., 2014; Tagliabue et al., 2019), defined
216 by the weighted average of all EEG electrodes that maximally discriminated hits from misses.
217 We first fitted the parameters of a detection model to these electrophysiological responses (Fig.
218 4B, S2) as well as to hit and false alarm rates (Fig. 4B, inset; Fig. S3). We then fitted two
219 additional parameters for confidence bias and sensitivity to observed confidence distributions.
220 The resulting model fitted the confidence ratings well (average R across participants 0.83 ± 0.03
221 for hits, 0.85 ± 0.03 for misses, 0.81 ± 0.04 for correct rejections and 0.45 ± 0.09 for false alarms;
222 Fig. 4C, S4), suggesting that evidence accumulation is a plausible mechanism underlying
223 perceptual consciousness and its electrophysiological correlates. The data and the model were
224 still consistent when stratifying per confidence level. Metacognitive sensitivity predicted by our
225 model and observed in the data were correlated for both “yes” responses ($R=0.60$, $p=0.001$,

226 permutation test) and “no” responses ($R=0.61$, $p=0.009$; Fig. 4E), showing that our model also
 227 successfully predicted metacognitive performance. Finally, an alternative model assuming that
 228 confidence for detected stimuli is sampled at a fixed latency after crossing the decision
 229 threshold and confidence for undetected stimuli is sampled from a random distribution led to a
 230 worse fit of the data ($BIC = 229.31 \pm 43.19$ compared to $BIC = 178.82 \pm 38.86$ for the maximal
 231 evidence model; $z = -2.33$, $p = 0.020$; Fig. 4F). This difference in goodness of fit was also
 232 observable in the correspondence between observed and simulated averaged confidence for
 233 hits ($R = 0.81 \pm 0.03$ for the maximal evidence model compared to $R = 0.63 \pm 0.09$ for the
 234 alternative model; $z = 2.29$; $p = 0.022$).



235 *Fig. 4. Computational model based on evidence accumulation. (A)* Time-varying drift rate (d ; thick black trace) had a
 236 short-lasting boost after a non-decision time following stimulus onset (dashed vertical line). Example evidence
 237 accumulation for one trial (EA; cyan trace for a hit, red trace for a miss) rises sharply after the drift boost and is
 238 attracted back to zero due to leakage. A stimulus is considered as perceived (hit) if EA reaches a decision threshold
 239 (horizontal line), and as non-perceived (miss) if not. The maximum of accumulated evidence with respect to the
 240 decision threshold is used as a confidence readout. *(B)* Model fit of the pEA locked on stimulus onset for hits (cyan trace)
 241 and misses (red trace). The corresponding observed EEG data is shown in grey. Average scalp topography of
 242 pEA weights is shown above. *(C)* Hit rate (HR) and false alarm rate (FAR). Datapoints are represented as ‘o’ and
 243 model simulations as ‘x’. *(D)* Left: Average confidence for hits (cyan), misses (red), correct rejections (green) and
 244 false alarms (black). Right: Model fits of the confidence distributions. Histograms show confidence distributions with
 245 95%-CI whiskers. Colored traces show model simulations. All shaded areas represent 95%-CI. *(E)* Area under the
 246 curve (AUC) correlation between observed data (horizontal axis) and simulated data (vertical axis) for “yes”
 247 responses (hits and false alarms; left) and “no” responses (correct rejections and misses; right). Regression line is
 248 shown in red with shaded areas representing 95%-CI. *(F)* Model comparison in terms of Bayesian information
 249 criterion (BIC) between the maximal evidence model and the alternative model. Whiskers represent 95%-CI and
 250 asterisk indicates statistical significance ($p < 0.05$).

251 Informed by our modelling results in healthy participants, we set out to verify whether we could
252 decode confidence for misses from single-neuron data in Experiment 2 using a decoder defining
253 confidence as the maximum of accumulated evidence. We took the best decoder for hits and
254 misses (trained on stimulus-locked data) and applied it out-of-sample across the stimulation
255 window (i.e. cue-locked). We decoded confidence for hits ($R = 0.49$, $p = 0.001$, permutation test)
256 and confidence for misses ($R = -0.31$, $p = 0.015$), which the aforementioned stimulus-locked
257 decoder could not achieve. The time corresponding to the decoded maximal evidence
258 correlated with stimulus onset for hits ($R = 0.37$, $p = 0.001$) but not for misses ($R = 0.03$, $p =$
259 0.58), suggesting that evidence for confidence in misses was not sampled synchronously with
260 the stimulus, thereby verifying the plausibility of the maximal evidence decoder on our patient's
261 single-neuron data.

262 Discussion

263 We propose a mechanism of evidence accumulation to explain the behavioral and neural
264 markers of perceptual consciousness and monitoring. We show that tactile detection relates to
265 an increase of the firing rate of single neurons in the posterior parietal cortex of a human
266 participant, as well as an increased scalp EEG response recorded in a group of healthy
267 participants. In both cases, the amplitude of the corresponding neural response was dependent
268 on the confidence in hits. This increase in neural response as well as in the detection reports
269 were well described by a computational model indicating that a plausible mechanism underlying
270 the building of confidence in both the presence and absence of a stimulus is for the brain to take
271 the maximal evidence accumulated over time.

272 *Encoding of detection by individual neurons in the posterior parietal cortex*

273 We had the opportunity to collect data from individual neurons in the human PPC, at the
274 junction between the postcentral and intraparietal sulcus in the superior parietal lobule. The
275 PPC has been associated with a multitude of functions linking perception to planning and action
276 (Andersen & Cui, 2009) and receives multisensory inputs including those from the primary
277 somatosensory cortex (Pearson & Powell, 1985). In Experiment 1, we found individual neurons
278 in the PPC with higher firing rates following detected stimuli. We argue that these neurons are
279 responsible for evidence accumulation based on the following three findings. Firstly, in
280 Experiment 1 we found neurons whose increase in firing rate for hits was synchronized to

281 response times (Gold & Shadlen, 2007). Secondly, in Experiment 1 the variance of the
282 corresponding spike rates increased after stimulus onset (Churchland et al., 2011). Thirdly, in
283 Experiment 3, we observed an increase in the firing rates for increasing intensities of (task-
284 irrelevant) stimuli (Gold & Shadlen, 2007). Based on these three hallmarks of evidence
285 accumulation, we argue that our results consist in the first single-neuron account of perceptual
286 evidence accumulation in a human subject capable of subjective reports. Indeed, although
287 electrophysiological correlates of evidence accumulation have been found in various regions of
288 non-human primate brains, including the frontal cortex or subcortical structures (Ding & Gold,
289 2010; Hanks et al., 2015; Odegaard et al., 2018), the arguably most common region studied in
290 relation with neural accumulation of perceptual evidence is the lateral intraparietal (LIP) area of
291 the PPC (Bolimunta & Ditterich, 2012; Katz et al., 2016; Roitman & Shadlen, 2002; Zhou &
292 Freedman, 2019). However, whether perceptual evidence accumulation neurons such as those
293 reported in non-human primate studies could support conscious reports is unclear, as subjective
294 experience cannot be measured explicitly in non-human species, and because such neurons
295 were – to our knowledge – not reported in humans yet.

296 *Encoding of confidence by individual neurons in the posterior parietal cortex*

297 In Experiment 2, we asked the participant again to detect stimuli and found neurons similar to
298 those in Experiment 1 with higher firing rates after stimuli reported as perceived. The finding of
299 detection-selective neurons when responses were provided by key press (Experiment 1) or
300 orally (Experiment 2) suggests that the mechanism of evidence accumulation we propose is
301 response-invariant. Importantly, we asked the participant to report the confidence he had in his
302 responses, and found that the change in firing rates for detected stimuli was modulated by
303 confidence, showing that confidence relates to the strength of single neuron's responses to
304 detected stimuli. This mechanistic overlap, which – to our knowledge – was not yet shown in
305 humans capable of reporting subjective confidence was confirmed at the neuronal population
306 level: multivariate decoders trained to discriminate hits vs. misses allowed us to decode
307 confidence for hits when time-locking to the stimulus onset and for both hits and misses when
308 locking on the onset of maximal evidence.

309 *Computational modelling and replication at the scalp level*

310 Because microelectrode implants in parietal regions are extremely rare in humans, we sought to
311 generalize our findings by recording behavioral and neural data in a group of healthy volunteers
312 in Experiment 4. Behavioral results revealed highly similar patterns between the two samples,

313 indicating that detection and confidence reports in Experiments 1-2 were not impacted by the
314 clinical condition. Experiment 4 also allowed us to generalize our single-neuron findings at a
315 larger scale based on EEG recordings. EEG data showed a similar dependence of detection-
316 related activity on confidence for hits, similar to previous work in the visual domain using a
317 different awareness scale (Tagliabue et al., 2019) and a discrimination task (Boldt & Yeung,
318 2015; Gherman & Philiastides, 2015). Of note, both neural responses recorded at the
319 intracranial (single-neuron, EcoG; Experiment 1-3) and scalp levels (Experiment 4) were
320 observed at a rather late latency following stimulus onset (>200 ms), suggesting that these
321 responses were not related to early somatosensory perceptual processes. We then reasoned
322 that since similar increases in neural activity are assumed to reflect accumulation of evidence
323 (O'Connell et al., 2012, 2018; Tagliabue et al., 2019), an evidence accumulation model should
324 predict both behavioral results (hit rate, false-alarm rate and confidence for hits, misses, correct
325 rejections and false-alarms) and corresponding neural responses. Using neural data to fit the
326 model instead of response times allowed us to fit a leakage parameter (Yu et al., 2015) and to
327 compensate for the fact that, in a detection task, response times are unavailable for undetected
328 stimuli. The model derives confidence as the distance between the maximal evidence
329 accumulated over time and the decision bound. This flexible readout provides a major
330 advantage when computing confidence in the absence of stimulus detection (i.e. misses) as well
331 as in the absence of a stimulus (i.e. correct rejections and false-alarms), which cannot be
332 achieved with models using decision-locked confidence readouts in discrimination tasks
333 (Pereira et al., 2020; Pleskac & Busemeyer, 2010; van den Berg et al., 2016). An alternative
334 model with a fixed-timing readout and a random confidence for unperceived stimuli performed
335 significantly worse. Our modelling results corroborate our electrophysiological results across
336 Experiments 1-4 and are consistent with decision-making models of confidence applied to
337 animal data, postulating a shared encoding of evidence for decision and confidence (Kiani &
338 Shadlen, 2009), possibly enriched by post-decisional evidence (Fleming et al., 2018; Pleskac &
339 Busemeyer, 2010; van den Berg et al., 2016). Moreover, a recent study comparing models
340 based on signal detection theory showed that the model that best fit observed data involves a
341 second-order "metacognitive" noise to the decisional evidence (Maniscalco & Lau, 2016). Our
342 model implicitly implements this metacognitive noise through the influence of first-order
343 parameters such as leakage on post-decisional evidence readouts. Indeed, in participant with
344 strong leakage, accumulated evidence rises and decays fast, leading to low metacognitive noise.
345 On the contrary, in participants with little leakage, once no more informative evidence is
346 accumulated, the level of evidence accumulation tends to oscillate around the reached

347 maximum, leading to higher metacognitive noise. A-posteriori analyses showed that the leakage
348 parameter correlated with metacognitive sensitivity (Supplementary information). Our model
349 thus provides a simple mechanism supporting metacognition, including subliminal stimuli,
350 explains neural responses and was verified at the single neuron and EEG level, as we were
351 able to decode confidence ratings above chance using this procedure.

352 *Implications for perceptual consciousness*

353 Our results posit that stimulus detectability involves the accumulation of sampled evidence
354 towards a decision bound, as previously discussed for discrimination tasks (Kang et al., 2017).
355 Of note, the use of a detection task is compatible with a contrastive study of consciousness
356 (Baars, 1998), as opposed to two-alternative forced choice discrimination tasks for which
357 confidence ratings are well characterized, but which do not offer a direct contrast between
358 perceived and unperceived stimuli. The view of conscious access as an all-or-none process
359 involving a decision bound is compatible with the ignition mechanism put forward by the global
360 workspace theory of consciousness (Mashour et al., 2020), according to which sufficiently
361 activated encapsulated networks may coalesce into a single network responsible for
362 broadcasting neural signals throughout the brain and thereby making them accessible to
363 conscious reports. One could speculate that the triggering of an ignition is governed by
364 bounded-evidence accumulation similar to the one operated by neuronal populations in the
365 posterior parietal cortex. Recently, the use of classical contrastive approaches to delineate the
366 neural correlates of consciousness has been criticized, on the basis that it may be confounding
367 the cognitive and neural mechanisms associated with phenomenal experience *per se*, and
368 those associated with reporting phenomenal experience (Aru et al., 2012). Some authors have
369 proposed the use of “no-report paradigms”, in which perceptual experience is not inferred from
370 participants’ responses, but from neural or peripheral signals while participants are passively
371 exposed to stimuli (Frassle et al., 2014; Tsuchiya et al., 2015; but see Block, 2019; Phillips &
372 Morales, 2020). Importantly, we found a population of neurons encoding perceptual evidence
373 through a putative evidence accumulation process in Experiment 3, in which the participant was
374 passively exposed to the stimuli similar to such no-report paradigms. Although these effects
375 were weaker than the ones found in Experiment 1-2, they indicate that evidence accumulation
376 operated by a neuronal population in the posterior parietal cortex is involved in conscious
377 perception, even when the stimuli are task-irrelevant. In addition, the mechanistic overlap
378 between detection and confidence we report cannot be due to similar motor responses
379 associated with detection and confidence reports in Experiment 2, as those were collected

380 separately, seconds after the end of the stimulation window on which our analysis was based in
381 the delayed detection task.

382 To conclude, our results posit that both detection and confidence for near-threshold stimuli
383 involve the accumulation of evidence towards a criterion orchestrated by the PPC. We argue
384 that this neuronal mechanism involving a decision bound may serve as a trigger for the neural
385 ignition underlying conscious access (Moutard et al., 2015; van Vugt et al., 2018) and explains
386 how contents remaining inaccessible to consciousness may still be subject to self-monitoring
387 (Mazor et al., 2020; Meuwese et al., 2014). Our behavioral, neural, and modeling results clarify
388 how perceptual consciousness and reflexive self-monitoring are intertwined mechanistically.

389 **References**

390 Andersen, R. A., & Cui, H. (2009). Intention, Action Planning, and Decision Making in Parietal-
391 Frontal Circuits. *Neuron*, 63(5), 568–583. <https://doi.org/10.1016/j.neuron.2009.08.028>

392 Aru, J., Axmacher, N., Do Lam, A. T. A., Fell, J., Elger, C. E., Singer, W., & Melloni, L. (2012).
393 Local Category-Specific Gamma Band Responses in the Visual Cortex Do Not Reflect
394 Conscious Perception. *Journal of Neuroscience*, 32(43), 14909–14914.
395 <https://doi.org/10.1523/JNEUROSCI.2051-12.2012>

396 Baars, B. J. (1998). Metaphors of consciousness and attention in the brain. *Trends in Cognitive
397 Sciences*, 21, 58–62.

398 Block, N. (2011). Perceptual consciousness overflows cognitive access. *Trends in cognitive
399 sciences*, 15(12), 567-575.

400 Block, N. (2019). What Is Wrong with the No-Report Paradigm and How to Fix It. *Trends in
401 Cognitive Sciences*, 23(12), 1003–1013. <https://doi.org/10.1016/j.tics.2019.10.001>

402 Bogacz, R., Brown, E., Moehlis, J., Holmes, P., & Cohen, J. D. (2006). The physics of optimal
403 decision making: A formal analysis of models of performance in two-alternative forced-
404 choice tasks. *Psychological Review*, 113(4), 700–765. [https://doi.org/10.1037/0033-295X.113.4.700](https://doi.org/10.1037/0033-
405 295X.113.4.700)

406 Boldt, A., & Yeung, N. (2015). Shared Neural Markers of Decision Confidence and Error
407 Detection. *Journal of Neuroscience*, 35(8), 3478–3484.
408 <https://doi.org/10.1523/JNEUROSCI.0797-14.2015>

409 Bollimunta, A., & Ditterich, J. (2012). Local Computation of Decision-Relevant Net Sensory
410 Evidence in Parietal Cortex. *Cerebral Cortex*, 22(4), 903–917.
411 <https://doi.org/10.1093/cercor/bhr165>

412 Brainard, D. H. (1997). The Psychophysics Toolbox. *Spatial Vision*, 10(4), 433–436.
413 <https://doi.org/10.1163/156856897X00357>

414 Brown, R., Lau, H., & LeDoux, J. E. (2019). Understanding the Higher-Order Approach to
415 Consciousness. *Trends in Cognitive Sciences*, 23(9), 754–768.
416 <https://doi.org/10.1016/j.tics.2019.06.009>

417 Busemeyer, Jerome R., T., James T. (1993). Decision field theory: A dynamic-cognitive
418 approach to decision making in an uncertain environment. *Psychological Review*, 100(3),
419 432–459.

420 Chalmers, D. J. (1995). Facing Up to the Problem of Consciousness. *Journal of Consciousness
421 Studies*, 2, 1–27.

422 Chaumon, M., Bishop, D. V. M., & Busch, N. A. (2015). A practical guide to the selection of
423 independent components of the electroencephalogram for artifact correction. *Journal of
424 Neuroscience Methods*, 250, 47–63. <https://doi.org/10.1016/j.jneumeth.2015.02.025>

425 Churchland, Anne. K., Kiani, R., Chaudhuri, R., Wang, X.-J., Pouget, A., & Shadlen, M. N.
426 (2011). Variance as a Signature of Neural Computations during Decision Making. *Neuron*,
427 69(4), 818–831. <https://doi.org/10.1016/j.neuron.2010.12.037>

428 Dehaene, S., & Changeux, J.-P. (2011). Experimental and Theoretical Approaches to
429 Conscious Processing. *Neuron*, 70(2), 200–227.
430 <https://doi.org/10.1016/j.neuron.2011.03.018>

431 Dehaene, S., Changeux, J.-P., Naccache, L., Sackur, J., & Sergent, C. (2006). Conscious,
432 preconscious, and subliminal processing: A testable taxonomy. *Trends in Cognitive*

433 *Sciences*, 10(5), 204–211. <https://doi.org/10.1016/j.tics.2006.03.007>

434 Dehaene, S., Charles, L., King, J.-R., & Marti, S. (2014). Toward a computational theory of
435 conscious processing. *Current Opinion in Neurobiology*, 25, 76–84.
436 <https://doi.org/10.1016/j.conb.2013.12.005>

437 Delorme, A., & Makeig, S. (2004). EEGLAB: An open source toolbox for analysis of single-trial
438 EEG dynamics including independent component analysis. *Journal of Neuroscience
439 Methods*, 134(1), 9–21. <https://doi.org/10.1016/j.jneumeth.2003.10.009>

440 Devine, C. A., Gaffney, C., Loughnane, G. M., Kelly, S. P., & O'Connell, R. G. (2019). The role
441 of premature evidence accumulation in making difficult perceptual decisions under
442 temporal uncertainty. *eLife*, 8, e48526. <https://doi.org/10.7554/eLife.48526>

443 Ding, L., & Gold, J. I. (2010). Caudate Encodes Multiple Computations for Perceptual Decisions.
444 *Journal of Neuroscience*, 30(47), 15747–15759.
445 <https://doi.org/10.1523/JNEUROSCI.2894-10.2010>

446 Flavell, J. H. (1979). Metacognition and cognitive monitoring: A new area of cognitive-
447 developmental inquiry. *American Psychologist*, 34(10), 906–911.

448 Fleming Stephen M., Dolan Raymond J. and Frith Christopher D. (2012) Metacognition:
449 computation, biology and function. *Phil. Trans. R. Soc. B* 367: 1280–1286

450 Fleming, S. M., & Lau, H. C. (2014). How to measure metacognition. *Frontiers in Human
451 Neuroscience*, 8. <https://doi.org/10.3389/fnhum.2014.00443>

452 Fleming, S. M., van der Putten, E. J., & Daw, N. D. (2018). Neural mediators of changes of mind
453 about perceptual decisions. *Nature Neuroscience*, 21(4), 617–624.
454 <https://doi.org/10.1038/s41593-018-0104-6>

455 Frassle, S., Sommer, J., Jansen, A., Naber, M., & Einhäuser, W. (2014). Binocular Rivalry:
456 Frontal Activity Relates to Introspection and Action But Not to Perception. *Journal of
457 Neuroscience*, 34(5), 1738–1747. <https://doi.org/10.1523/JNEUROSCI.4403-13.2014>

458 Fu, Z., Wu, D.-A. J., Ross, I., Chung, J. M., Mamelak, A. N., Adolphs, R., & Rutishauser, U.
459 (2019). Single-Neuron Correlates of Error Monitoring and Post-Error Adjustments in
460 Human Medial Frontal Cortex. *Neuron*, 101(1), 165–177.e5.
461 <https://doi.org/10.1016/j.neuron.2018.11.016>

462 Gherman, S., & Philippi, M. G. (2015). Neural representations of confidence emerge from
463 the process of decision formation during perceptual choices. *NeuroImage*, 106, 134–143.
464 <https://doi.org/10.1016/j.neuroimage.2014.11.036>

465 Gold, J. I., & Shadlen, M. N. (2007). The Neural Basis of Decision Making. *Annual Review of
466 Neuroscience*, 30(1), 535–574. <https://doi.org/10.1146/annurev.neuro.29.051605.113038>

467 Groppe, D. M., Bickel, S., Dykstra, A. R., Wang, X., Mégevand, P., Mercier, M. R., Lado, F. A.,
468 Mehta, A. D., & Honey, C. J. (2017). iELVis: An open source MATLAB toolbox for
469 localizing and visualizing human intracranial electrode data. *Journal of Neuroscience
470 Methods*, 281, 40–48. <https://doi.org/10.1016/j.jneumeth.2017.01.022>

471 Hanks, T. D., Kopec, C. D., Brunton, B. W., Duan, C. A., Erlich, J. C., & Brody, C. D. (2015).
472 Distinct relationships of parietal and prefrontal cortices to evidence accumulation. *Nature*,
473 520(7546), 220–223. <https://doi.org/10.1038/nature14066>

474 Herding, J., Ludwig, S., von Lautz, A., Spitzer, B., & Blankenburg, F. (2019). Centro-parietal
475 EEG potentials index subjective evidence and confidence during perceptual decision
476 making. *NeuroImage*, 201, 116011. <https://doi.org/10.1016/j.neuroimage.2019.116011>

477 Kamiński, J., Sullivan, S., Chung, J. M., Ross, I. B., Mamelak, A. N., & Rutishauser, U. (2017).
478 Persistently active neurons in human medial frontal and medial temporal lobe support
479 working memory. *Nature Neuroscience*, 20(4), 590–601. <https://doi.org/10.1038/nn.4509>

480 Kang, Y. H. R., Petzschner, F. H., Wolpert, D. M., & Shadlen, M. N. (2017). Piercing of
481 Consciousness as a Threshold-Crossing Operation. *Current Biology*, 27(15), 2285–
482 2295.e6. <https://doi.org/10.1016/j.cub.2017.06.047>

483 Katz, L. N., Yates, J. L., Pillow, J. W., & Huk, A. C. (2016). Dissociated functional significance of
484 decision-related activity in the primate dorsal stream. *Nature*, 535(7611), 285–288.
485 <https://doi.org/10.1038/nature18617>

486 Kiani, R., & Shadlen, M. N. (2009). Representation of Confidence Associated with a Decision by
487 Neurons in the Parietal Cortex. *Science*, 324(5928), 759–764.
488 <https://doi.org/10.1126/science.1169405>

489 Kleiner, M. (n.d.). *What's new in Psychtoolbox-3?* 89.

490 Koch, C., Massimini, M., Boly, M., & Tononi, G. (2016). Neural correlates of consciousness:
491 Progress and problems. *Nature Reviews Neuroscience*, 17(5), 307–321.
492 <https://doi.org/10.1038/nrn.2016.22>

493 Koriat, A. (2006). Metacognition and consciousness. In *The Cambridge Handbook of
494 Consciousness* (Vol. 3, pp. 289–326).

495 Kvam, P. D., Pleskac, T. J., Yu, S., & Busemeyer, J. R. (2015). Interference effects of choice on
496 confidence: Quantum characteristics of evidence accumulation. *Proceedings of the
497 National Academy of Sciences*, 112(34), 10645–10650.
498 <https://doi.org/10.1073/pnas.1500688112>

499 Lamme, V. A. F. (2010). How neuroscience will change our view on consciousness. *Cognitive
500 Neuroscience*, 1(3), 204–220. <https://doi.org/10.1080/17588921003731586>

501 Lau, H., & Rosenthal, D. (2011). Empirical support for higher-order theories of conscious
502 awareness. *Trends in Cognitive Sciences*, 15(8), 365–373.
503 <https://doi.org/10.1016/j.tics.2011.05.009>

504 Li, Q., Hill, Z., & He, B. J. (2014). Spatiotemporal Dissociation of Brain Activity Underlying
505 Subjective Awareness, Objective Performance and Confidence. *Journal of Neuroscience*,
506 34(12), 4382–4395. <https://doi.org/10.1523/JNEUROSCI.1820-13.2014>

507 Makeig, S., Bell, A. J., Jung, T.-P., & Sejnowski, T. J. (n.d.). *Independent Component Analysis
508 of Electroencephalographic Data*. 7.

509 Maniscalco, B., & Lau, H. (2016). The signal processing architecture underlying subjective
510 reports of sensory awareness. *Neuroscience of Consciousness*, 2016(1).
511 <https://doi.org/10.1093/nc/niw002>

512 Mashour, G. A., Roelfsema, P., Changeux, J. P., & Dehaene, S. (2020). Conscious processing
513 and the global neuronal workspace hypothesis. *Neuron*, 105(5), 776–798.

514 Mazor, M., Friston, K. J., & Fleming, S. M. (2020). Distinct neural contributions to metacognition
515 for detecting, but not discriminating visual stimuli. *eLife*, 9, e53900.
516 <https://doi.org/10.7554/eLife.53900>

517 Meuwese, J. D. I., van Loon, A. M., Lamme, V. A. F., & Fahrenfort, J. J. (2014). The subjective
518 experience of object recognition: Comparing metacognition for object detection and object
519 categorization. *Attention, Perception, & Psychophysics*. <https://doi.org/10.3758/s13414-014-0643-1>

521 Moutard, C., Dehaene, S., & Malach, R. (2015). Spontaneous Fluctuations and Non-linear
522 Ignitions: Two Dynamic Faces of Cortical Recurrent Loops. *Neuron*, 88(1), 194–206.
523 <https://doi.org/10.1016/j.neuron.2015.09.018>

524 Nagel, T. (1974). What is it like to be a bat. *The Philosophical Review*, 4, 435–450.

525 O'Connell, R. G., Dockree, P. M., & Kelly, S. P. (2012). A supramodal accumulation-to-bound
526 signal that determines perceptual decisions in humans. *Nature Neuroscience*, 15(12),
527 1729–1735. <https://doi.org/10.1038/nn.3248>

528 Odegaard, B., Grimaldi, P., Cho, S. H., Peters, M. A. K., Lau, H., & Basso, M. A. (2018).
529 Superior colliculus neuronal ensemble activity signals optimal rather than subjective
530 confidence. *Proceedings of the National Academy of Sciences*, 115(7), E1588–E1597.
531 <https://doi.org/10.1073/pnas.1711628115>

532 Pearson, R., & Powell, T. (1985). The projection of the primary somatic sensory cortex upon
533 area 5 in the monkey. *Brain Research Reviews*, 9(1), 89–107.
534 [https://doi.org/10.1016/0165-0173\(85\)90020-7](https://doi.org/10.1016/0165-0173(85)90020-7)

535 Pelli, D. G. (1997). The VideoToolbox software for visual psychophysics: Transforming numbers
536 into movies. *Spatial Vision*, 10(4), 437–442.

537 Pereira, M., Faivre, N., Iturrate, I., Wirthlin, M., Serafini, L., Martin, S., Desvachez, A., Blanke,
538 O., Van De Ville, D., & Millán, J. del R. (2020). Disentangling the origins of confidence in
539 speeded perceptual judgments through multimodal imaging. *Proceedings of the National
540 Academy of Sciences*, 117(15), 8382–8390. <https://doi.org/10.1073/pnas.1918335117>

541 Philiastides, M. G., Heekeren, H. R., & Sajda, P. (2014). Human Scalp Potentials Reflect a
542 Mixture of Decision-Related Signals during Perceptual Choices. *Journal of Neuroscience*,
543 34(50), 16877–16889. <https://doi.org/10.1523/JNEUROSCI.3012-14.2014>

544 Phillips, I., & Morales, J. (2020). The Fundamental Problem with No-Cognition Paradigms.
545 *Trends in Cognitive Sciences*, 24(3), 165–167. <https://doi.org/10.1016/j.tics.2019.11.010>

546 Pitts, M. A., Padwal, J., Fennelly, D., Martínez, A., & Hillyard, S. A. (2014). Gamma band activity
547 and the P3 reflect post-perceptual processes, not visual awareness. *NeuroImage*, 101,
548 337–350. <https://doi.org/10.1016/j.neuroimage.2014.07.024>

549 Pleskac, T. J., & Busemeyer, J. R. (2010). Two-stage dynamic signal detection: A theory of
550 choice, decision time, and confidence. *Psychological Review*, 117(3), 864–901.
551 <https://doi.org/10.1037/a0019737>

552 Quiroga, R. Q., Mukamel, R., Isham, E. A., Malach, R., & Fried, I. (2008). Human single-neuron
553 responses at the threshold of conscious recognition. *Proceedings of the National
554 Academy of Sciences*, 105(9), 3599–3604. <https://doi.org/10.1073/pnas.0707043105>

555 Ratcliff, R., & Van Dongen, H. P. A. (2011). Diffusion model for one-choice reaction-time tasks
556 and the cognitive effects of sleep deprivation. *Proceedings of the National Academy of
557 Sciences*, 108(27), 11285–11290. <https://doi.org/10.1073/pnas.1100483108>

558 Ratcliff, Roger, & Rouder, J. N. (n.d.). *A Diffusion Model Account of Masking in Two-Choice
559 Letter Identification*. 14.

560 Reber, T. P., Faber, J., Niediek, J., Boström, J., Elger, C. E., & Mormann, F. (2017). Single-
561 Neuron Correlates of Conscious Perception in the Human Medial Temporal Lobe. *Current
562 Biology*, 27(19), 2991-2998.e2. <https://doi.org/10.1016/j.cub.2017.08.025>

563 Roitman, J. D., & Shadlen, M. N. (2002). Response of Neurons in the Lateral Intraparietal Area
564 during a Combined Visual Discrimination Reaction Time Task. *The Journal of*

565 *Neuroscience*, 22(21), 9475–9489. <https://doi.org/10.1523/JNEUROSCI.22-21-09475.2002>

566 Rutishauser, U., Aflalo, T., Rosario, E. R., Pouratian, N., & Andersen, R. A. (2018). Single-
567 Neuron Representation of Memory Strength and Recognition Confidence in Left Human
568 Posterior Parietal Cortex. *Neuron*, 97(1), 209-220.e3.
569 <https://doi.org/10.1016/j.neuron.2017.11.029>

570 Rutishauser, U., Schuman, E. M., & Mamelak, A. N. (2006). Online detection and sorting of
571 extracellularly recorded action potentials in human medial temporal lobe recordings, in
572 vivo. *Journal of Neuroscience Methods*, 154(1–2), 204–224.
573 <https://doi.org/10.1016/j.jneumeth.2005.12.033>

574 Rutishauser, U., Ye, S., Koroma, M., Tudusciuc, O., Ross, I. B., Chung, J. M., & Mamelak, A. N.
575 (2015). Representation of retrieval confidence by single neurons in the human medial
576 temporal lobe. *Nature Neuroscience*, 18(7), 1041–1050. <https://doi.org/10.1038/nn.4041>

577 Salti, M., Monto, S., Charles, L., King, J.-R., Parkkonen, L., & Dehaene, S. (2015). Distinct
578 cortical codes and temporal dynamics for conscious and unconscious percepts. *eLife*, 4,
579 e05652. <https://doi.org/10.7554/eLife.05652>

580 Savitzky, Abraham., & Golay, M. J. E. (1964). Smoothing and Differentiation of Data by
581 Simplified Least Squares Procedures. *Analytical Chemistry*, 36(8), 1627–1639.
582 <https://doi.org/10.1021/ac60214a047>

583 Shea, N., & Frith, C. D. (2019). The Global Workspace Needs Metacognition. *Trends in
584 Cognitive Sciences*, 23(7), 560–571. <https://doi.org/10.1016/j.tics.2019.04.007>

585 Tagliabue, C. F., Veniero, D., Benwell, C. S. Y., Cecere, R., Savazzi, S., & Thut, G. (2019). The
586 EEG signature of sensory evidence accumulation during decision formation closely tracks
587 subjective perceptual experience. *Scientific Reports*, 9(1), 4949.
588 <https://doi.org/10.1038/s41598-019-41024-4>

589 Tsuchiya, N., Wilke, M., Frässle, S., & Lamme, V. A. F. (2015). No-Report Paradigms:
590 Extracting the True Neural Correlates of Consciousness. *Trends in Cognitive Sciences*,
591 19(12), 757–770. <https://doi.org/10.1016/j.tics.2015.10.002>

592 van den Berg, R., Anandalingam, K., Zylberberg, A., Kiani, R., Shadlen, M. N., & Wolpert, D. M.
593 (2016). A common mechanism underlies changes of mind about decisions and confidence.
594 *eLife*, 5, e12192. <https://doi.org/10.7554/eLife.12192>

595 van Vugt, B., Dagnino, B., Vartak, D., Safaai, H., Panzeri, S., Dehaene, S., & Roelfsema, P. R.
596 (2018). The threshold for conscious report: Signal loss and response bias in visual and
597 frontal cortex. *Science*, 360(6388), 537–542. <https://doi.org/10.1126/science.aar7186>

598 Wyart, V., & Tallon-Baudry, C. (2009). How Ongoing Fluctuations in Human Visual Cortex
599 Predict Perceptual Awareness: Baseline Shift versus Decision Bias. *Journal of
600 Neuroscience*, 29(27), 8715–8725. <https://doi.org/10.1523/JNEUROSCI.0962-09.2009>

601 Zeki, S. (2007). The disunity of consciousness. In *Progress in Brain Research* (Vol. 168, pp. 11–
602 268). Elsevier. [https://doi.org/10.1016/S0079-6123\(07\)68002-9](https://doi.org/10.1016/S0079-6123(07)68002-9)

603 Zhou, Y., & Freedman, D. J. (2019). Posterior parietal cortex plays a causal role in perceptual
604 and categorical decisions. *Science*, 180–185.

605

606 STAR METHODS

607 KEY RESSOURCE TABLE

REAGENT or RESSOURCE	SOURCE	IDENTIFIER
Software and Algorithms		
MATLAB 2018a	MathWorks	RRID:SCR_001622; http://www.mathworks.com/products/matlab/
Osort		RRID:SCR_015869; http://www.rutishauserlab.org/osort
EEGLAB 2019.1.0		RRID:SCR_007292; http://sccn.ucsd.edu/eeglab/index.html
iELVis		RRID:SCR_016109; http://ielvis.pbworks.com/w/page/116347253/FrontPage
Psychophysics toolbox 3		RRID:SCR_002881; http://psychtoolbox.org/
Algorithm to fit an evidence accumulation model to behavioral and neural data		Upon acceptance
Other		
Neuroport recording system	Blackrock Microsystems	https://www.blackrockmicro.com/
Brain Quick LTM	Micromed	http://www.micromed.eu/en-us/
WaveGuard EEG	ANTNeuro	http://www.ant-neuro.com

608 CONTACT FOR REAGENT AND RESSOURCE SHARING

609 Further information and requests for ressources should be addressed directly to the Lead Contact,
610 Nathan Faivre (nathan.faivre@univ-grenoble-alpes.fr)

611 EXPERIMENTAL MODEL AND SUBJECT DETAILS

612 In experiments 1–3, the participant was a 23-year-old right-handed man suffering from drug-resistant
613 epilepsy due to a focal cortical dysplasia in the left central sulcus. As part of the clinical management of
614 his condition, he received a 4x6 ECoG grid covering the left premotor, motor, sensory and posterior
615 parietal cortices. He accepted to participate in a clinical trial on neuronal recordings during invasive
616 epilepsy monitoring at the Geneva University Hospitals (IN-MAP; NCT02932839) and a Utah
617 microelectrode array was additionally implanted in the left posterior parietal cortex. The patient provided

618 informed written consent and the study was approved by the Commission Cantonale d'Ethique de la
619 Recherche de la République et Canton de Genève (2016-01856). Eighteen healthy participants (7
620 females; age: 25.2 years, SD = 4.1) took part in Experiment 4 for a monetary compensation. Participants
621 gave written informed consent prior to participating and all experimental procedures were approved by
622 the Commission Cantonale d'Ethique de la Recherche de la République et Canton de Genève (2015-
623 00092 15-273).

624 **METHOD DETAILS**

625 Experimental paradigms were written in Matlab (Mathworks) using the Psychophysics toolbox (Brainard,
626 1997; Kleiner, n.d.; Pelli, 1997). In all experiments, stimuli were applied on the lateral palmar side of the
627 right wrist using a MMC3 Haptuator vibrotactile device from TactileLabs Inc. (Montréal, Canada) driven by
628 a 230 Hz sinusoid audio signal lasting 100 ms. Experiments started by a simple estimation of the
629 individual detection threshold. The tactile stimulus was applied with decreasing intensity with steps
630 corresponding to 2% of the initial intensity until the participant reported not feeling it anymore three times
631 in a row. We then repeated the same procedure but with increasing intensity and until the participant
632 reported feeling the vibration three times in a row. The perceptual threshold was estimated to be the
633 average between the two thresholds found using this procedure. This approximation was then used as a
634 seed value for an adaptive staircase during the main experiments (see below). Experiments 1-3 were
635 performed on different days at the patient's bedside.

636 **Experiment 1**

637 Stimuli were applied in a pseudo-random way with an inter-stimulus interval of two seconds plus an
638 exponentially distributed time (mean: 2 s). The participant was provided with a keypad and asked to press
639 a key every time he felt a stimulus. Answers provided during the two seconds following a stimulus were
640 considered as hits. Only one keypress occurred out of this two second post-stimulus window.

641 **Experiment 2**

642 An auditory cue signaled the start of the two seconds stimulus window during which the stimulus could be
643 applied at any time (uniform distribution) in 80% of trials (the remaining 20% served as catch trials,
644 unbeknownst to the participant). Stimulus onset was followed by a one second delay to ensure that
645 stimulus-locked activity was not contaminated by the detection response. After this delay, a second
646 auditory cue probed the participant for his detection response ("yes" or "no"), followed by a three levels
647 confidence rating (1: "unsure", 2: "somewhat sure", 3: "very sure"). Detection and confidence ratings were
648 provided vocally and registered by the experimenter.

649 **Experiment 3**

650 Stimuli were applied in a pseudo-random way with an inter-stimulus interval of two seconds plus an
651 exponentially distributed time (mean: 2 s) with a random amplitude sampled from 11 intensities ranging
652 from zero to five times the participant's perceptual threshold. The participant was not given any
653 instructions and was left free to mind-wander during the experiment.

654 **Experiment 4**

655 Participants sat in front of a computer screen. A white fixation cross appeared in the middle of the screen
656 for 2 s. From the moment the fixation cross turned green, participants were told that a tactile stimulus
657 could be applied at any moment during the next 2 s. During this period, stimulus onset was uniformly
658 distributed in 80% of trials, the 20% remaining trials served as catch trials, as in Experiment 2. In all trials,
659 1 second after the green cross disappeared, participants were prompted to answer with the keyboard
660 whether they felt the stimulus or not. Following a 500 ms stimulus onset asynchrony, participants were
661 asked to report the confidence in their first order response by moving a slider on a visual analog scale
662 with marks at 0 (certainty that the first-order response was erroneous), 0.5 (unsure about the first-order
663 response) and 1.0 (certainty that the first-order response was correct). Detection and confidence reports
664 were provided with the left (non-stimulated) hand, using different keys. The total experiment included 500
665 trials divided in 10 blocks, and lasted about 2 hours.

666 **Electrophysiological data acquisition**

667 A 96-channel silicon-based microelectrode array ("Utah array"; Blackrock Microsystems, Salt Lake City,
668 USA) was implanted in the posterior parietal cortex, immediately posterior to the postcentral sulcus and
669 the hand representation of sensorimotor cortex (Fig. 1A). The location was confirmed through post-hoc
670 electrode localization (Fig. 1G), performed through a coregistration of a preoperative MRI structural T1
671 scan and a postoperative CT scan using the iELVIS toolbox (Groppe et al., 2017). The data from each of
672 the 96 channels was amplified and sampled at 30 KHz for offline analysis (NeuroPort system, Blackrock
673 Microsystems LLC, Salt Lake City, USA). Additionally, a 24 electrode ECoG grid (Ad-Tech Medical)
674 covered the left hemisphere from the premotor cortex to the superior parietal lobule (Fig.1G, 2D). The
675 data was amplified and sampled at 2048 Hz (Brain Quick LTM, Micromed, Treviso, Italy). In Experiment 4,
676 electroencephalographic data were acquired from 62 active electrodes (10-20 montage) using a
677 WaveGuard EEG cap and amplifier (ANTNeuro, Hengelo, The Netherlands) and digitized at a sampling
678 rate of 1024 Hz. Horizontal and vertical electrooculography (EOG) was derived using bipolar referenced
679 electrodes placed around participants' eyes. The audio signal driving the vibrotactile actuator was
680 recorded as an extra channel to precisely realign data to stimulus onset.

681 **QUANTIFICATION AND STATISTICAL ANALYSIS**

682 **Invasive electrophysiological data processing and univariate analysis**

683 The raw signal from the microelectrode array was bandpass filtered between 300 and 3000 Hz for spike
684 sorting. Trials with epileptic activity or other artifacts were removed from further analysis following visual
685 inspection of ECoG data. Spikes were extracted and sorted using the semi-automatic template matching
686 'Osorth' algorithm (Rutishauser et al., 2006). Standard quality metrics were computed for each putative
687 single unit in order to assess their quality (Fig. S1). We computed the firing rate every 1ms with a 100 ms
688 standard deviation Gaussian sliding window.

689 In Experiment 1, a neuron was considered detection-selective when a significant (two-sided test) effect of
690 detection was found on the number of spikes during a time window between 0.5 and 1.5 seconds after
691 stimulus onset using a generalized linear model (GLM) with a Poisson distribution (Fu et al., 2019;
692 Rutishauser et al., 2018). For this, we fitted a model with one beta regressor: $\#spikes \sim \beta_0 + \beta_1 * detection$
693 (hit or miss). For the latency analysis, we computed the cumulative sum of spikes starting at stimulus
694 onset and correlated (Spearman) it with RTs for every time step (1 ms) between 0 and 1.5 s after stimulus
695 onset. A neuron was considered RT-selective if the correlation was significant within this time range after
696 correcting for false-discovery rate (FDR). To ensure that there was no overfitting and that our results were
697 not driven by outliers, we used a non-parametric permutation test to assess whether the number of
698 selective neurons was significantly above chance; we repeatedly (N=1000) applied the same tests on
699 shuffled data and counted the number of selective neurons. We defined the p-value as the proportion of
700 times that the number of selective neurons for shuffled data was higher than the number of selective
701 neurons found in the data (Fu et al., 2019; Kamiński et al., 2017; Rutishauser et al., 2018). When no
702 selective neuron was found in the shuffled data, we set $p = 1/N = 0.001$. In Experiment 2, we also used a
703 Poisson GLM to regress the number of spikes during a time window between 0.5 and 1.5 seconds after
704 stimulus onset. We fitted a model with three beta regressors: $\#spikes \sim \beta_0 + \beta_1 * detection +$
705 $\beta_2 * confidence + \beta_3 * detection * confidence$. We only interpreted main effects (β_1, β_2) in the absence of
706 interactions (β_3). If β_3 was significant (two-sided test), we considered the neuron as detection- and
707 confidence-selective. If β_1 was significant but β_3 was not, we considered the neuron only detection-
708 selective (idem for confidence-selective). We applied the same permutation test as for Experiment 1. In
709 Experiment 3, we fitted a Poisson GLM with one beta regressors: $\#spikes \sim \beta_0 + \beta_1 * intensity$ to find
710 intensity-selective neurons showing an increased firing rate with increasing stimulus intensity and applied
711 the same permutation test as for Experiment 1 and 2.

712 For ECoG analyses, we re-referenced the channels to a common average and applied a lowpass filter
713 (Hamming window with a cutoff frequency of 40 Hz). Trials with epileptic activity or other artifacts were
714 removed from further analysis following visual inspection. We used linear models (LM) for statistics using
715 the same regressors as for spike counts (see above). For display purposes only, we additionally
716 smoothed the data with a 200 ms Savitzky-Golay filter (Savitzky & Golay, 1964).

717 **Analysis of variance for Experiment 1**

718 To further relate our results to evidence accumulation, we analyzed some typical signatures of drift
719 diffusion-like processes: the variance in the number of spikes during an epoch can be decomposed into i)
720 the variance of the point process expected if the neuron had a constant firing rate across trials, and ii) the
721 remaining variance of the conditional expectation (VarCE) which is due to the variability of the neuron's
722 underlying firing rate across trials. If neuronal activity follows a diffusion process, then VarCE should
723 increase with decision time. Similarly, the correlation between conditional expectations (CorCE) should be
724 stronger between adjacent time windows and decrease with time lag between time windows (Churchland
725 et al., 2011). We followed the approach in Churchland and colleagues. In brief, we relied on an upper
726 bound estimate of VarCE, assuming that the point process variance is proportional to the spike count so:

727
$$s^2 = Var_{CE} + \phi \bar{N},$$

728 with s^2 the total variance and \bar{N} the average number of spikes for one 50 ms epoch. We used 10 non-
729 overlapping epochs ranging from 0 to 1.5 s post-stimulus. The variance of the point process was
730 computed as is a weighted average of the variance of the point process for hits and for misses. The
731 constant ϕ can be set based on some heuristics such as by considering that VarCE is zero when the ratio
732 of variance and mean firing rate is minimal (e.g. at the beginning of the decision process). Due to the
733 limited number of trials available in this study, we preferred this approach to more complex methods
734 involving data fitting.

735 We computed CorCE by dividing the covariance of the number of spikes for different epochs by the
736 square root of the product of the VarCE:

737
$$Cor_{CE}^{ij} = Cov^{ij} / \sqrt{Var_{CE}^i * Var_{CE}^j},$$

738 with Cov^{ij} the covariance between epoch i and j and Var_{CE}^i the VarCE for epoch i. For all computations,
739 we reduced ϕ by 20% to have positive semi-definite covariance matrices.

740 **Multivariate decoding (Experiment 2)**

741 We fed single neurons firing rates sampled every 10 ms into linear discriminant decoders with a L2
742 regularization factor of 0.8 (similar results were obtained with different regularization factors). These
743 decoders separated the space of input features with a linear hyperplane that best discriminates hits and
744 misses. The decoders predict a hit when the distance of a sample to the separating hyperplane is higher
745 than zero and a miss otherwise. To avoid overfitting, we separated our data in 10 cross-validation folds so
746 that for each fold we trained decoders on the 90% of the data and tested them on the 10% remaining (i.e.

747 out-of-sample). The distance to the separating hyperplane was also used to compute the area under the
748 curve (AUC) for out-of-sample data at each time point. We used permutation tests to assess whether
749 similar AUC could have been obtained by chance while correcting for multiple comparisons across time
750 points. We selected contiguous clusters of time points when AUC was higher than 0.6 or lower than 0.4
751 and then computed the proportion of similar or bigger clusters obtained with shuffled labels. For each
752 permutation, we computed AUC clusters over the whole set of time points to keep the autocorrelation
753 structure in the shuffled data.

754 Confidence was decoded at the time point corresponding to the highest AUC. Decoded confidence was
755 defined as the absolute distance of a sample to the separating hyperplane. We assessed confidence
756 decoding by correlating (Spearman) decoded confidence with observed confidence and assessing
757 significance using permutation tests (one-sided, as we could reasonably expect positive correlations). As
758 this procedure was carried out on out-of-sample data, our results were not affected by overfitting. Finally,
759 for maximal evidence decoding, we used the same decoder to decode firing rates between 0.5 and 3 s
760 post-cue. We excluded the first 0.5 s due to some neurons showing post-cue activity. We then took the
761 maximum of the decoder over that time window, correlated it with confidence observed in the data and
762 assessed significance using permutation tests (one-sided). Again, this procedure was carried out on out-
763 of-sample data so our results cannot be affected by overfitting.

764 **Scalp EEG data preprocessing (Experiment 4)**

765 All channels were high-pass filtered using a Hamming window with a cutoff frequency of 0.1 Hz. We
766 defined an epoch as the 3 seconds of data centered around the event corresponding to the vibrotactile
767 stimuli recorded using an auxiliary channel. EEG and EOG data were then lowpass filtered using a
768 Hamming window with a cutoff frequency of 40 Hz and visually inspected to remove trials and channels
769 containing artifacts. We computed the independent component analysis (ICA) (Makeig et al., 1996) on a
770 copy of the EEG epochs that were highpass filtered at 1Hz. The number of independent components (ICs)
771 computed corresponded to 99% of the variance, which resulted in 14.78 ± 1.27 ICs per subject. We used
772 SASICA (Chaumon et al., 2015) with default parameters to automatically select ICs for rejection and
773 visually inspected all components scheduled for rejection before actually rejecting them. IC weights kept
774 were then back-projected to the original EEG epochs. Any channel rejected prior to the ICA was
775 reinterpolated using spherical interpolation ($N = 0.67 \pm 0.23$, max 3). Finally, we visually inspected all
776 channels and rejected artifactual epochs. All pre-processing was done with the EEGLAB toolbox
777 (Delorme & Makeig, 2004). The final dataset comprised 464.17 ± 13.73 epochs per subject.

778 To assess which electrodes were detection- and/or confidence-selective, we used a linear mixed model to
779 regress single-trial average EEG responses in the 0.5 to 1.5 time-window used for single-neuron analysis.
780 For each electrode, we tried different random factors and kept the model with the lowest Bayesian

781 Information Criterion. P-values were Bonferroni corrected for multiple comparisons. To compute the
782 electrophysiological correlate of evidence accumulation, we sought to find the best weighting of EEG
783 electrodes in terms of discriminability between hits and misses. For this, we trained decoders of hits
784 versus misses between -0.5 and 1.5 s from stimulus onset with 20 ms steps in a 10-fold cross-validation
785 scheme. We repeated this procedure 10 times and searched for the time point with highest average
786 discriminability. We then retrained one decoder using the EEG at this time point and used the weights of
787 this decoder to construct one single value at every time point, representing a proxy to the amount of
788 evidence for hits. We baselined this proxy signal using the 300 ms pre-stimulus.

789 **Ornstein-Uhlenbeck bounded accumulation model**

790 To test whether the observed electrophysiological correlate of conscious detection could index evidence
791 accumulation, we used an Ornstein–Uhlenbeck process which consists of a drift diffusion model with a
792 leakage parameter driving the accumulated evidence back to zero (Busemeyer & Townsend, 1993). The
793 model consisted of an evidence accumulation process $EA(t)$ integrating a time-varying drift rate $d(t)$ with a
794 leakage factor λ plus additive white noise $W(t)$ with a fixed standard deviation of $\sigma = 0.1$ (Eq. 1). The
795 evidence accumulation process $EA(t)$ was bounded by zero to be more biologically plausible (since firing
796 rates are positive).

$$797 EA(t + 1) = \max([1 - \lambda * dt] * EA(t) + d(t) + \sigma W(t), 0) \\ 798 \quad (1)$$

799 To model temporal uncertainty, the accumulation process started at the beginning of the stimulus window
800 (Devine et al., 2019) with a drift of zero and ended 3 s later, as in our experimental paradigm. On stimulus
801 onset, and after a non-decision time (ndt), the drift rate $d(t)$ rose to a level γ for 100 ms (stimulus duration)
802 and then decayed exponentially with a factor k (Eq. 2). We used the same distribution of stimulus onsets
803 as in the data (from 0 to 2 s after the cue). To model variability in the drift rate for a detection task (Ratcliff
804 & Van Dongen, 2011), γ was sampled from a half-normal distribution with mean γ_{μ} and standard
805 deviation γ_{σ} (i.e. absolute value of a normal distribution). This allowed us to have variability in the drift
806 rate while keeping it positive.

$$807 d(t) = \begin{cases} 0 & \text{if } t < s + ndt \\ 1 & \text{if } (s + ndt) \leq t \leq (s + ndt + 0.1) \\ v(t) & \text{if } t > (s + ndt + 0.1), \quad v(t) = \gamma e^{[t-s-ndt-0.1/k]^2} \end{cases} \quad (2)$$

808 With s the onset of the stimulus. Stimuli were considered to be detected if the accumulated evidence
809 reached a decision bound θ .

810 Confidence $c(t)$ was simulated as the accumulated evidence $EA(t)$, scaled by a factor α and shifted by a
811 factor β (confidence bias), inverted if the decision bound was not reached ($\text{invert}(x) = 1 - x$) before being
812 saturated to the 0 - 1 interval by a sigmoidal function (Pereira et al., 2020) (Eq. 3). The time at which
813 confidence $c(t)$ was read-out corresponded to the maximum of $EA(t)$ over the 3s stimulation time window.
814 Of note, we expressed the confidence readout in percentage of the decision bound. This scaling did not
815 affect simulated confidence but normalized the readout across participants and helped restrain the grid
816 search for good initial parameters.

817
$$c(t) = e^{\alpha*EA(t)+\beta} / (e^{\alpha*EA(t)+\beta} + 1) \quad (3)$$

818 **Model fitting**

819 We used a two-stage fitting procedure: We first fitted the parameters of the decisional process to
820 detection responses and to the pEA described above and then fitted a second set of parameters to
821 predict confidence ratings.

822 In the first stage, we simulated ($N=500$) trials of $EA(t)$ along with the corresponding detection responses.
823 The objective function of the optimization procedure was based on the likelihood of the model with
824 respect to the hit rate and false-alarm rate observed in the data and the shape of the average of $pEA(t)$
825 for hits and misses. Since our model is agnostic to the scale of $pEA(t)$ and $EA(t)$, we scaled them both by
826 their average over time and realizations (trials or simulations). The log-likelihood thus corresponded to the
827 normal probability of observing such a hit-rate and false-alarm rate and the normal probability of
828 observing such an electrophysiological response for hits and misses. We used a Nelder-Mead simplex
829 optimization with 756 different initial parameters sampling a broad range of values for γ_μ , γ_σ , λ and k .
830 For each such iteration, we first did a grid search on ndt and θ to find plausible starting values. We kept
831 the parameters corresponding to the model with the best likelihood. To ensure a good fit, we did a final
832 fitting with $N=10'000$ simulated trials.

833 In the second stage, we also simulated ($N=500$) trials of $EA(t)$ along with the corresponding detection
834 responses and used these to simulate confidence ratings. We used a Kolmogorov-Smirnov test for the
835 log-likelihood of confidence for hits, misses and correct rejections. We used a Nelder-Mead simplex
836 optimization with 66 different initial parameters sampling a broad range of values for α and β . We kept
837 the parameters corresponding to the model with the best likelihood. To ensure a good fit, we did a final
838 fitting with $N=10'000$ simulated trials.

839 **Metacognitive sensitivity**

840 We evaluated metacognitive sensitivity or how well confidence predicted task performance (Fleming &
841 Lau, 2014). For this, we assessed the relation between confidence ratings and detection accuracy using

842 the area under the curve, computed independently for “yes” responses (hits and false alarms) and “no”
843 responses (correct rejections and misses) (Mazor et al., 2020; Meuwese et al., 2014)

844 **Alternative model**

845 We compared our maximal evidence model with an alternative model which assumed that confidence
846 was readout at a fixed timing (t_{RO}) post-decision for perceived stimuli. For unperceived stimuli (i.e. with
847 no decision), this alternative model assumed that participants reported random confidence estimates,
848 based on Gaussian noise with mean Ω and unit standard deviation. As in the maximal evidence model,
849 confidence corresponded to evidence scaled by a factor α and shifted by a factor β (confidence bias)
850 before being saturated to the 0 - 1 interval by a sigmoidal function. The model thus comprised four
851 parameters: α , β , t_{RO} and Ω which were fitted with the same procedure as for the maximal evidence
852 model, except that the grid search for optimal initial parameters was extended to include two initial values
853 for t_{RO} : 0.25 and 0.5 s. We used the Bayesian Information Criterion to compare the two models.

854 **DATA AND SOFTWARE AVAILABILITY**

855 Behavioral, electrocorticographic and electroencephalographic data with the corresponding analyses
856 scripts will be made available upon publication. Single-neuron data are available upon request.